DOI 10.1007/s10946-023-10150-w
*Journal of Russian Laser Research, Volume 44, Number 4, July, 2023*

# BEAM PROPAGATION FACTOR OF A PARTIALLY COHERENT TWISTED ELLIPTICAL VORTEX BEAM IN INHOMOGENEOUS ATMOSPHERIC TURBULENCE

**Wenli Liu, Yonggen Xu,* Bangzhuo An, Qian Xu, Nianchi Hao, and Yongtao Liu**

*Department of Physics, School of Science*
*Key Laboratory of High-Performance Scientific Computation, Xihua University*
*Chengdu 610039, China*

*Corresponding author e-mail: xuyonggen06@126.com

**Abstract**

Based on the extended Huygens–Fresnel principle and the second-order moments of the Wigner distribution function (WDF), we derive the analytical formulas for the root-mean-square (rms) spatial width, rms angular width, and $M^2$-factor of a partially coherent twisted elliptical vortex beam (PCTEVB) propagating through the inhomogeneous atmospheric turbulence. The spatial spreading, angular width, and $M^2$-factor of a PCTEVB in turbulence are investigated numerically and comparatively. We find an interesting result that the relative rms angular width and $M^2$-factor of PCTEVB with a small ellipticity propagating through turbulence decreases, meaning that the elliptical vortex beam is less affected by the inhomogeneous atmospheric turbulence in comparison with the traditional vortex beam. We also find that the relative $M^2$-factor and the relative rms angular width of PCTEVB mainly depend on the topological charge, twist factor, initial coherent length, zenith angle, and propagation distance. In addition, the PCTEVB, with a small initial coherent length and ellipticity as well as a large twist factor, has a stronger anti-turbulence ability. Our outcomes may have future extensive possibilities in free-space optical communications.

**Keywords:** PCTEVB, inhomogeneous atmospheric turbulence, ellipticity, twist factor, angular width, $M^2$-factor.

## 1. Introduction

In the past decades, partially coherent (PC) beams attract more and more attention. They have been studied extensively in both theory and experiment due to its stronger anti-turbulence ability than fully coherent beam in the turbulent atmosphere and it has been found their stronger advantage in widely practical applications in free space optical communication, active laser radar systems, optical imaging, and remote sensing [1–10]. Twisted partially coherent (TPC) beam is one of the most known kinds of PC beams, which carries the twist phase, and was first introduced by Simon [11]. Past researches have shown that TPC beams can reduce some physics phenomenon (e.g., the beam spot, quantum information processing, etc.) caused by atmospheric turbulence on the propagation [4, 9, 12–20]. Furthermore, the partially coherent vortex (PCV) beams are also commonly used and have been studied widely [6]. In 1992, Allen [21] first found the vortex beams, which can carry the $m\hbar$ orbital angular momentum (OAM), where $m$ is the topological charge carried by the beams, and $\hbar$ is the reduced Planck's constant. Also, the

Manuscript submitted by the authors in English on May 6, 2023.

 

beams carrying the vortex phase can reduce the beam wander and the turbulent-induced scintillation [1, 3,6,9,12,21–30]. In short, the TPC beams and the PCV beams have strong anti-turbulence ability, when the beam carries the twist phase and the vortex phase simultaneously, in particular [4, 12].

On the other hand, it is well known that researchers divided the atmospheric turbulence into homogeneous atmospheric turbulence and inhomogeneous atmospheric turbulence. The formation of atmospheric turbulence is caused by the existence of many airflow vortices with different basic physical properties in the flowing atmosphere, which keeps moving and changing [31, 32]. The strength of atmospheric turbulence is described by the structure constant of the refractive index fluctuations of the turbulence $C_n^2$, which is a function of space and time [31, 32]. In addition, atmospheric turbulence can be classified as strong turbulence, medium turbulence, and weak turbulence with the method of dividing the intensity of the atmospheric turbulence proposed by Davis [33]. Compared with homogeneous atmospheric turbulence, the $C_n^2$ of inhomogeneous atmospheric turbulence is not constant but varies with altitude, geographical location, etc. [33–35]. In recent researches, the fluctuation of atmospheric turbulence will cause the speckle effect, light intensity scintillation, beam expansion, phase distortion, and so on [36–40]. To some extent, this seriously affects the beam quality and restricts the application of lasers. Hence, studying the propagation factor of the laser beam in inhomogeneous atmospheric turbulence is meaningful.

However, to the best of our knowledge, the propagation factor of partially coherent twisted elliptical vortex beam (PCTEVB) through inhomogeneous atmospheric turbulence have not been studied so far. Therefore, in this paper, we obtain the theoretical formulas of PCTEVB and study the influences of the propagation factors. The results exhibit that the PCTEVB has better propagation properties and stronger anti-turbulence ability than the traditional vortex beam. In addition, these results can provide references for the practical applications of laser beams.

## 2. Theory

The optical field distribution of PCTEVB at the plane of incidence is shown as follows [41–43]:

$$E(x', y'; 0) = \left[\frac{x'}{w_{0x}} - i\,\mathrm{sign}(m)\frac{y'}{w_{0y}}\right]^{|m|} \exp\left(-\frac{x'^2}{w_{0x}^2} - \frac{y'^2}{w_{0y}^2}\right), \tag{1}$$

where $\rho' = (x', y')$ represents radial coordinates in the incident plane, $w_{0x}$ and $w_{0y}$ are the beam waist sizes of PCTEVB in the $x'$ and $y'$ directions, respectively, $\mathrm{sign}(\cdot)$ is a sign function: when $m > 0$, $\mathrm{sign}(m) = 1$, when $m = 0$, $\mathrm{sign}(m) = 0$, and when $m < 0$, $\mathrm{sign}(m) = -1$, with $m$ being the topological charge.

The cross-spectral density (CSD) of PCTEVB at the source plane reads

$$W(x_1', x_2', y_1', y_2'; 0) = \left\langle E(x_1', y_1'; 0)E^*(x_2', y_2'; 0)\right\rangle_m = \left(\frac{x_1'}{w_{0x}} - i\,\mathrm{sign}(m)\frac{y_1'}{w_{0y}}\right)^{|m|}$$
$$\times \left(\frac{x_2'}{w_{0x}} + i\,\mathrm{sign}(m)\frac{y_2'}{w_{0y}}\right)^{|m|} \exp\left(-\frac{x_1'^2 + x_2'^2}{w_{0x}^2} - \frac{y_1'^2 + y_2'^2}{w_{0y}^2}\right) \exp\left[-\frac{(x_1' - x_2')^2 + (y_1' - y_2')^2}{2\delta_0^2}\right], \tag{2}$$

where $\rho_n' = (x_n', y_n')$; $n = 1, 2$ represents any position vector defined on the incident plane, $\delta_0$ is the initial correlation length, $\langle\cdot\rangle_m$ denotes the ensemble average, and $^*$ describes the complex conjugate.

Based on the extended Huygens–Fresnel principle with a paraxial form, the CSD of PCTEVB propagating through the inhomogeneous atmospheric turbulence can be given by [44–47]

$$W(\rho,\rho_d;z)=\left(\frac{1}{\lambda z}\right)^2\iiiint W(\rho',\rho_d';0)\times\exp\left[\frac{ik}{z}(\rho-\rho')\cdot(\rho_d-\rho_d')-H(\rho_d,\rho_d';z)\right]d^2\rho'\,d^2\rho_d', \quad (3)$$

where the central coordinate systems at the source plane can be listed as $\rho'=(x',y')$ and $\rho_d'=(x_d',y_d')$, the accepting plane can be written as $\rho=(x,y)$ and $\rho_d=(x_d,y_d)$, while $\rho_n=(x_n,y_n)$; $n=1,2$ are the arbitrary position vectors defined on the accepting plane, $k=2\pi/\lambda$ is the wave number, with $\lambda$ being the wavelength, and $z$ is the propagation distance of PCTEVB in the inhomogeneous atmospheric turbulence [36, 37, 45, 46]. Also, here,

$$\begin{aligned} x'&=\frac{x_1'+x_2'}{2}, \qquad y'=\frac{y_1'+y_2'}{2}, \qquad x_d'=x_1'-x_2', \qquad y_d'=y_1'-y_2',\\ x&=\frac{x_1+x_2}{2}, \qquad y=\frac{y_1+y_2}{2}, \qquad x_d=x_1-x_2, \qquad y_d=y_1-y_2. \end{aligned} \quad (4)$$

In Eq. (3), $\exp[-H(\rho_d,\rho_d';z)]$ represents the contribution of the inhomogeneous atmospheric turbulence, and the $H$ can be given as follows [33, 34, 44, 45]:

$$H(\rho_d,\rho_d';z)=\frac{4\pi^2k^2}{\cos(\gamma)}\int_{h_0}^{H_0}dh\int_0^\infty\left\{1-J_0[\kappa|\zeta\rho_d'+(1-\zeta)\rho_d|]\right\}\Phi_n(\kappa,h)\kappa\,d\kappa, \quad (5)$$

where $\gamma$ is the zenith angle, $h$ is the propagation height, $H_0$ represents the ground height of the received plane, and $h_0$ denotes the ground height of the light source plane, if we take $h_0=0$; it means that the light source plane is on the ground. Also, here, $J_0(\cdot)$ is the zero-order Bessel function of the first kind, $\zeta=1-(h-h_0)/[z\cos(\gamma)]$ denotes the normalized distance variable and $z=(H_0-h_0)/\cos(\gamma)$, $\Phi_n(\kappa,h)=C_n^2(h)\Phi_n'(\kappa)$ represents the spatial power spectrum of the refractive-index fluctuations of inhomogeneous atmospheric turbulence, $\kappa$ is the spatial wave number, and $C_n^2(h)$ is the generalized refractive-index structure parameter, with units $\mathrm{m}^{3-\alpha}$ varying with $h$.

It is well known that the Winger distribution function (WDF) of the PC beam on propagation can be given by the formula [35–37, 44–46]

$$h(\rho,\theta,z)=\left(\frac{k}{2\pi}\right)^2\iint W(\rho,\rho_d;z)\exp(-ik\theta\cdot\rho_d)d^2\rho_d, \quad (6)$$

where $\theta=(\theta_x,\theta_y)$ is the rms angular width, and $W(\rho,\rho_d;z)$ can be rewritten as [35–40, 44–46]

$$\begin{aligned} W(\rho,\rho_d;z)&=\left(\frac{1}{2\pi}\right)^2\\ &\times\iiiint W\left(\rho'',\rho_d+\frac{z}{k}\kappa_d;0\right)\times\exp\left[-i\rho\cdot\kappa_d+i\kappa_d\cdot\rho''-H\left(\rho_d,\rho_d+\frac{z}{k}\kappa_d;z\right)\right]d^2\kappa_d\,d^2\rho'', \end{aligned} \quad (7)$$

with $\kappa_d=(\kappa_{dx},\kappa_{dy})$ being the position vector in the spatial–frequency domain. Further, we can obtain the expression of $H(\rho_d,\rho_d+z/k\kappa_d;z)$ as [5, 44–46]

$$H\left(\rho_d,\rho_d+\frac{z}{k}\kappa_d;z\right)=\frac{4\pi^2k^2}{\cos\gamma}\int_{h_0}^{H_0}dh\int_0^\infty\left[1-J_0\left(\kappa\left|\zeta\frac{z}{k}\kappa_d+\rho_d\right|\right)\right]\Phi_n(\kappa,h)\kappa\,d\kappa. \quad (8)$$

Hence, we arrive at the expression of the CSD of PCTEVB beam in the $z = 0$ plane; it reads

$$W\left(\rho'', \rho_d + \frac{z}{k}\kappa_d; 0\right) = \left[\frac{1}{w_{0x}^2}(x''^2 - x_d'^2/4) + \frac{1}{w_{0y}^2}(y''^2 - y_d'^2/4) - \frac{i\,\mathrm{sign}(m)}{w_{0x}w_{0y}}(x''y_d' - x_d'y'')\right]^{|m|}$$
$$\times \exp\left[-\frac{1}{w_{0x}^2}(2x''^2 + x_d'^2/2) - \frac{1}{w_{0y}^2}(2y''^2 + y_d'^2/2) - \frac{x_d'^2 + y_d'^2}{2\delta_0^2}\right] \times \exp[ik\mu_0(x''y_d' - x_d'y'')], \tag{9}$$

where $\rho'' = (x'', y'')$, $\rho_d + \kappa_d z/k = (x_d', y_d')$, $\mu_0$ represents the twist factor of PCTEVB. For the convenience of calculation, in this paper, we take $m = +1$ and $-1$.

Based on the definition of intensity moment for WDF, the $n_1 + n_2 + m_1 + m_2$ order moments of WDF on the received plane for three-dimensional beams are [35–37, 44–46]

$$\langle x^{n_1} y^{n_2} \theta_x^{m_1} \theta_y^{m_2} \rangle = \frac{1}{P} \iint x^{n_1} y^{n_2} \theta_x^{m_1} \theta_y^{m_2} h(\rho, \theta; z) d^2\rho\, d^2\theta, \tag{10}$$

where $P = \iint h(\rho, \theta; z)\, d^2\rho\ d^2\theta$ is the total power of the beam.

In Eq. (10), if $n_1 = 2$ and $n_2 = m_1 = m_2 = 0$, the second-order moment $\langle x^2 \rangle$ of the beam on the receiving plane after transmission in atmosphere reads

$$\langle x^2 \rangle = \frac{1}{P} \iint x^2(\rho, \theta, z)\ d^2\rho\ d^2\theta. \tag{11}$$

Similarly, we can get some other second-order moments: $\langle y^2 \rangle$, $\langle x\theta_x \rangle$, $\langle y\theta_y \rangle$, $\langle \theta_x^2 \rangle$, and $\langle \theta_y^2 \rangle$.

Therefore, some second-order moments of PCTEVB in the incident plane $z = 0$ are

$$\langle \eta^2 \rangle_0 = \frac{1}{P} \iint \eta^2 W(\rho', 0; 0)\ d^2\rho', \tag{12}$$

$$\langle \theta_\eta^2 \rangle_0 = -\frac{1}{Pk^2} \iint \frac{\partial^2}{\partial \eta_d^2} [W(\rho', \eta_d; 0)]_{\eta_d = 0}\ d^2\rho', \tag{13}$$

$$\langle \eta\theta_\eta \rangle_0 = -\frac{i}{Pk} \iint \frac{\partial}{\partial \eta_d} [\eta W(\rho', \eta_d; 0)]_{\eta_d = 0}\ d^2\rho', \tag{14}$$

where $\langle \cdot \rangle_0$ represents the second-order moment at the plane $z = 0$, $\eta = x$ or $y$.

Thus, we arrive at the final calculation, namely,

$$\langle \rho^2 \rangle = \langle x^2 \rangle + \langle y^2 \rangle = Az^2 + \frac{w_{0y}^2}{2\beta^2}(1 + \beta^2) + T_1(z, \gamma), \tag{15}$$

$$\langle \rho \cdot \theta \rangle = \langle x\theta_x \rangle + \langle y\theta_y \rangle = Az + T_2(z, \gamma), \tag{16}$$

$$\langle \theta^2 \rangle = \langle \theta_x^2 \rangle + \langle \theta_y^2 \rangle = A + T_3(z, \gamma), \tag{17}$$

$$A = \left[\frac{2}{k^2 w_{0y}^2} + \frac{\mu_0^2 w_{0y}^2}{2\beta^2} - \mathrm{sign}(m)\frac{\mu_0}{k\beta}\right](1 + \beta^2) + \frac{2}{k^2\delta_0^2}, \tag{18}$$

where $\beta = w_{0y}/w_{0x}$ is ellipticity, and $T_1(z,\gamma)$, $T_2(z,\gamma)$, and $T_3(z,\gamma)$ represent the inhomogeneous atmospheric turbulence. The expressions are [5, 44]

$$T_1(z,\gamma) = \frac{4\pi^2 z^2}{\cos\gamma}\int_0^\infty \Phi_n'(\kappa)\kappa^3\, d\kappa \int_0^{z\cos\gamma}\left(1-\frac{h}{z\cos\gamma}\right)^2 C_n^2(h)\, dh, \tag{19}$$

$$T_2(z,\gamma) = \frac{4\pi^2 z}{\cos\gamma}\int_0^\infty \Phi_n'(\kappa)\kappa^3\, d\kappa \int_0^{z\cos\gamma}\left(1-\frac{h}{z\cos\gamma}\right) C_n^2(h)\, dh, \tag{20}$$

$$T_3(z,\gamma) = \frac{4\pi^2}{\cos\gamma}\int_0^\infty \Phi_n'(\kappa)\kappa^3\, d\kappa \int_0^{z\cos\gamma} C_n^2(h)\, dh. \tag{21}$$

Here, $\gamma$ is the zenith angle, $C_n^2(h)$ represents the refractive index structure parameter, and $\Phi_n'(\kappa)$ is non-Kolmogorov power spectrum.

Based on the second-order moments of the WDF, the spatial spreading and the rms angular width of the PCTEVB propagating through the inhomogeneous turbulent atmosphere read

$$w(z,\gamma) = (\langle\rho^2\rangle)^{1/2} = \left[Az^2 + \frac{w_{0y}^2}{2\beta^2}(1+\beta^2) + T_1(z,\gamma)\right]^{1/2}, \tag{22}$$

$$\theta(z,\gamma) = (\langle\theta^2\rangle)^{1/2} = [A + T_3(z,\gamma)]^{1/2}. \tag{23}$$

The beam transmission factor is an important index used to evaluate the beam quality. Based on the WDF, we can give expression of $M^2$-factor; it is

$$\begin{aligned} M^2(z,\gamma) &= k\left(\langle\rho^2\rangle\langle\theta^2\rangle - \langle\rho\cdot\theta\rangle^2\right)^{1/2} \\ &= k\left\{\left[Az^2 + \frac{w_{0y}^2}{2\beta^2}(1+\beta^2) + T_1(z,\gamma)\right]\times[A + T_3(z,\gamma)] - [Az + T_2(z,\gamma)]^2\right\}^{1/2}. \end{aligned} \tag{24}$$

In this paper, the non-Kolmogorov power spectrum is used as a model for inhomogeneous atmospheric turbulence, and we can give its spatial power spectrum $\Phi_n(\kappa,h)$ as follows [5, 44]:

$$\Phi_n(\kappa,h) = C_n^2(h)\frac{A(\alpha)}{(\kappa^2+\kappa_0^2)^{\alpha/2}}\exp\left(-\frac{\kappa^2}{\kappa_m}\right) = C_n^2(h)\Phi_n'(\kappa), \tag{25}$$

where $\kappa_0 = 2\pi/L_0$, with $L_0$ being the outer scale of atmospheric turbulence, and $\kappa_m = c(\alpha)/l_0$, with $l_0$ being the inner scale of atmospheric turbulence.

According to the Hufnagel–Valley (H-V) model proposed, $C_n^2(h)$ can be given as [5, 44]

$$C_n^2(h) = 0.00549\left(\frac{v}{27}\right)^2(10^{-5}h)^{10}\exp\left(\frac{-h}{1000}\right) + 2.7\cdot10^{-16}\exp\left(\frac{-h}{1500}\right) + 1.7\cdot10^{-14}\exp\left(\frac{-h}{100}\right), \tag{26}$$

where $v = 21$ m/s is the wind speed.

After substituting Eq. (26) into Eqs. (19)–(21), respectively, we arrive at the inhomogeneous atmo-

spheric turbulence quantities $T_1$, $T_2$, and $T_3$; they read

$$T_1(z,\gamma) = \frac{A(\alpha)\pi^2}{0.3322(\alpha-2)}\left\{[2\kappa_0^2\kappa_m^{2-\alpha} + (\alpha-2)\kappa_m^{4-\alpha}]\exp\left(\frac{\kappa_0^2}{\kappa_m^2}\right)\Gamma\left(2-\frac{\alpha}{2},\frac{\kappa_0^2}{\kappa_m^2}\right) - 2\kappa_0^{4-\alpha}\right\}$$
$$\times\Big\{\frac{z^2v^2}{\cos\gamma}\exp\left(\frac{-z\cos\gamma}{1000}\right)\left[-1.9645\cdot10^{-43}\sum_{n=1}^{9}\frac{n(n+1)}{(11-n)!}(z\cos\gamma)^{9-n}10^{3n} - \frac{2.1609\cdot10^{-11}}{z\cos\gamma}\right]$$
$$+\frac{1}{\cos^3\gamma}\left[-2.5931\cdot10^{-8}\exp\left(\frac{-z\cos\gamma}{1000}\right)v^2 - 1.2109\cdot10^{-6}\exp\left(\frac{-z\cos\gamma}{1500}\right)\right]$$
$$+\frac{1}{\cos^3\gamma}\left[-2.259\cdot10^{-8}\exp\left(\frac{-z\cos\gamma}{100}\right) + 2.5931\cdot10^{-8}v^2 + 1.2335\cdot10^{-6}\right]$$
$$+\frac{z}{\cos^2\gamma}\left(-4.3219\cdot10^{-12}v^2 - 1.03315\cdot10^{-9}\right) + \frac{z^2}{\cos\gamma}\cdot1.39858\cdot10^{-12}\Big\}, \qquad (27)$$

$$T_2(z,\gamma) = \frac{A(\alpha)\pi^2}{0.3322(\alpha-2)}\left\{[2\kappa_0^2\kappa_m^{2-\alpha} + (\alpha-2)\kappa_m^{4-\alpha}]\exp\left(\frac{\kappa_0^2}{\kappa_m^2}\right)\Gamma\left(2-\frac{\alpha}{2},\frac{\kappa_0^2}{\kappa_m^2}\right) - 2\kappa_0^{4-\alpha}\right\}$$
$$\times\Big\{\frac{zv^2}{\cos\gamma}\exp\left(\frac{-z\cos\gamma}{1000}\right)\cdot1.9645\cdot10^{-46}\sum_{n=0}^{10}\frac{n}{(11-n)!}(z\cos\gamma)^{10-n}10^{3n}$$
$$+\frac{1}{\cos^2\gamma}\left[2.161\cdot10^{-12}\exp\left(\frac{-z\cos\gamma}{1000}\right)v^2 + 4.0362\cdot10^{-10}\exp\left(\frac{-z\cos\gamma}{1500}\right)\right]$$
$$+\frac{1}{\cos^2\gamma}\left[1.1259\cdot10^{-10}\exp\left(\frac{-z\cos\gamma}{100}\right) - 2.161\cdot10^{-12}v^2 - 5.1657\cdot10^{-10}\right]$$
$$+\frac{z^2}{\cos\gamma}1.39858\cdot10^{-12}\Big\}, \qquad (28)$$

and

$$T_3(z,\gamma) = \frac{A(\alpha)\pi^2}{0.3322(\alpha-2)}\left\{[2\kappa_0^2\kappa_m^{2-\alpha} + (\alpha-2)\kappa_m^{4-\alpha}]\exp\left(\frac{\kappa_0^2}{\kappa_m^2}\right)\Gamma\left(2-\frac{\alpha}{2},\frac{\kappa_0^2}{\kappa_m^2}\right) - 2\kappa_0^{4-\alpha}\right\}$$
$$\times\Big\{\frac{v^2}{\cos\gamma}\left[\exp\left(\frac{-z\cos\gamma}{1000}\right)\cdot(-1.9645\cdot10^{-46})\sum_{n=0}^{10}\frac{1}{(10-n)!}(z\cos\gamma)^{10-n}10^{3n} + 1.9645\cdot10^{-16}\right]$$
$$+\frac{1}{\cos\gamma}\left[-2.6908\cdot10^{-13}\exp\left(\frac{-z\cos\gamma}{1500}\right) - 1.1295\cdot10^{-12}\exp\left(\frac{-z\cos\gamma}{100}\right) + 1.39858\cdot10^{-12}\right]\Big\}. \qquad (29)$$

To compare, we define the spatial spreading, the rms angular width and the relative $M^2$-factor of PCTEVB in inhomogeneous atmospheric turbulence as follows:

$$w_r(z,\gamma) = \frac{w(z,\gamma)}{w_f(z)}, \qquad \theta_r(z,\gamma) = \frac{\theta(z,\gamma)}{\theta_f(z)}, \qquad M_r^2(z,\gamma) = \frac{M^2(z,\gamma)}{M_f^2(z)}. \qquad (30)$$

In Eq. (30), $w_f(z)$, $\theta_f(z)$, and $M^2f(z)$ represent the spatial spreading, the rms angular width, and the $M^2$-factor of PCTEVB, respectively, in free space.

On the other hand, in Eq. (9), for the sake of convenience in calculation, the topological charge $m$ is taken to be either $+1$ or $-1$. When $m$ takes other integer values, we substitute Eq. (9) into Eq. (10) and, using the same method, after tedious derivation, arrive at the second-order moment of PCTEVB on the receiving plane,

$$\langle \rho^2 \rangle = \frac{(m+1)w_{0y}^2}{4\beta^2}(1+\beta^2) + \left[ \left( \frac{m+1}{k^2 w_{0y}^2} + \frac{m+1}{4\beta^2}\mu_0^2 w_{0y}^2 - \frac{m\mu_0}{k\beta} \right)(1+\beta^2) + \frac{2}{k^2\delta_0^2} \right] z^2 + T_1(z,\gamma), \quad (31)$$

$$\langle \rho \cdot \theta \rangle = \left[ \left( \frac{m+1}{k^2 w_{0y}^2} + \frac{m+1}{4\beta^2}\mu_0^2 w_{0y}^2 - \frac{m\mu_0}{k\beta} \right)(1+\beta^2) + \frac{2}{k^2\delta_0^2} \right] z + T_2(z,\gamma), \quad (32)$$

$$\langle \theta^2 \rangle = \left( \frac{m+1}{k^2 w_{0y}^2} + \frac{m+1}{4\beta^2}\mu_0^2 w_{0y}^2 - \frac{m\mu_0}{k\beta} \right)(1+\beta^2) + \frac{2}{k^2\delta_0^2} + T_3(z,\gamma). \quad (33)$$

## 3. Discussion

We fixed some parameters: $\lambda = 632.8$ nm, $k = 2\pi/\lambda$, $\alpha = 3.2$, $l_0 = 10$ mm, $L_0 = 100$ m, and $v = 21$ m/s [5, 44, 47]. Unless otherwise stated, these values are used as the calculation parameters.

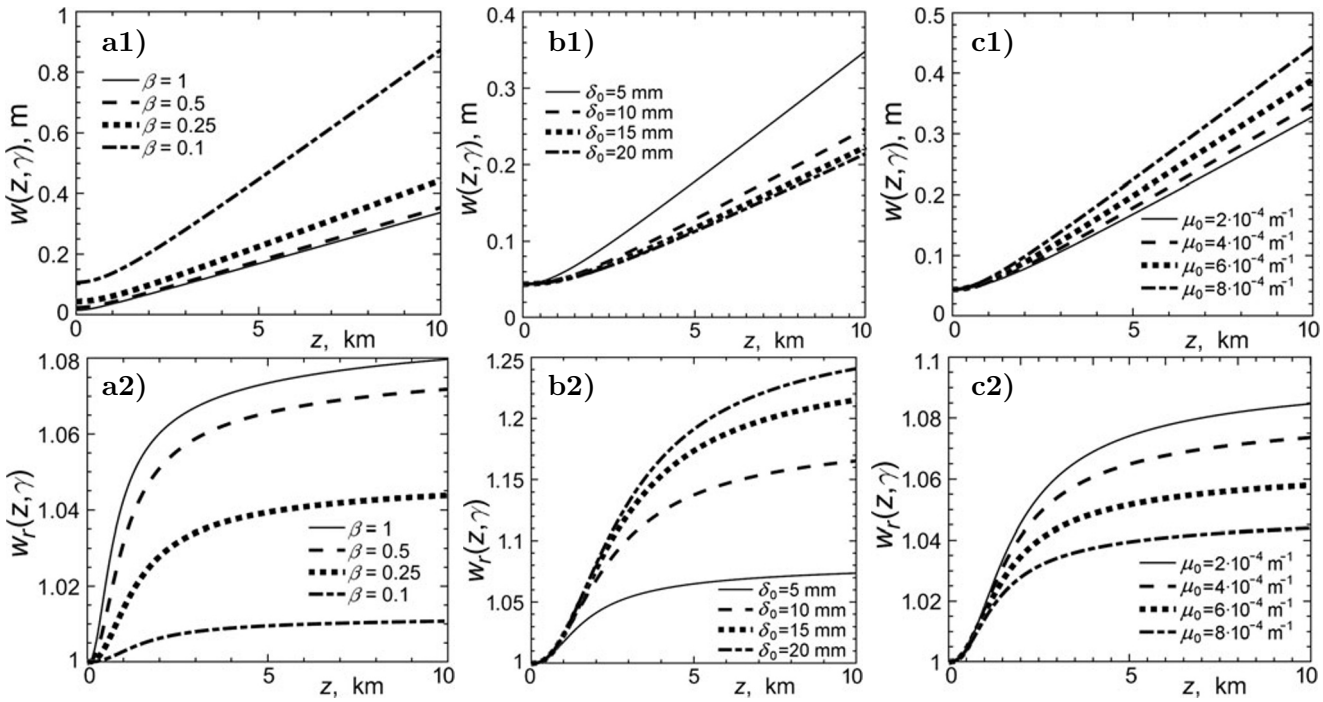


**Fig. 1.** The spatial spreading $w(z,\gamma)$ and relative spatial spreading $w_r(z,\gamma)$ of PCTEVB under different beam parameters versus the propagation distance through inhomogeneous turbulent atmosphere. Here, $m = 1$ and $\gamma = \pi/3$; also, $\mu_0 = 8 \cdot 10^{-4}$ m$^{-1}$ and $\delta_0 = 5$ mm (a1, a2); $\mu_0 = 4 \cdot 10^{-4}$ m$^{-1}$ and $\beta = 0.25$ (b1, b2); $\beta = 0.25$ and $\delta_0 = 5$ mm (c1, c2).

In Fig. 1, we illustrate the spatial spreading and the relative spatial spreading of PCTEVB through inhomogeneous atmospheric turbulence under different ellipticity $\beta$, twist factors $\mu_0$, and the initial

coherent lengths $\delta_0$ versus the propagation distance. In Fig. 1, we can see that both the spatial spreading and the relative spatial spreading are becoming larger with increase in the propagation distance, then they are close to saturation. In the other words, the effect of atmospheric turbulence on PCTEVB is weaken with increase in the propagation distance. In addition, in Fig. 1 a1, b1, c1, we see that the spatial spreading of PCTEVB decreases with decrease of the twist factor and increase in the ellipticity and the initial coherent length. However, one can also find in Fig. 1 a2, b2, c2 that the relative spatial spreading decreases for PCTEVB with decrease of the ellipticity and the initial coherent length and increase in the twist factor. This indicates that it is less affected by the inhomogeneous atmospheric turbulence in the case of beams with smaller ellipticity and initial coherent length, and a larger twist factor.

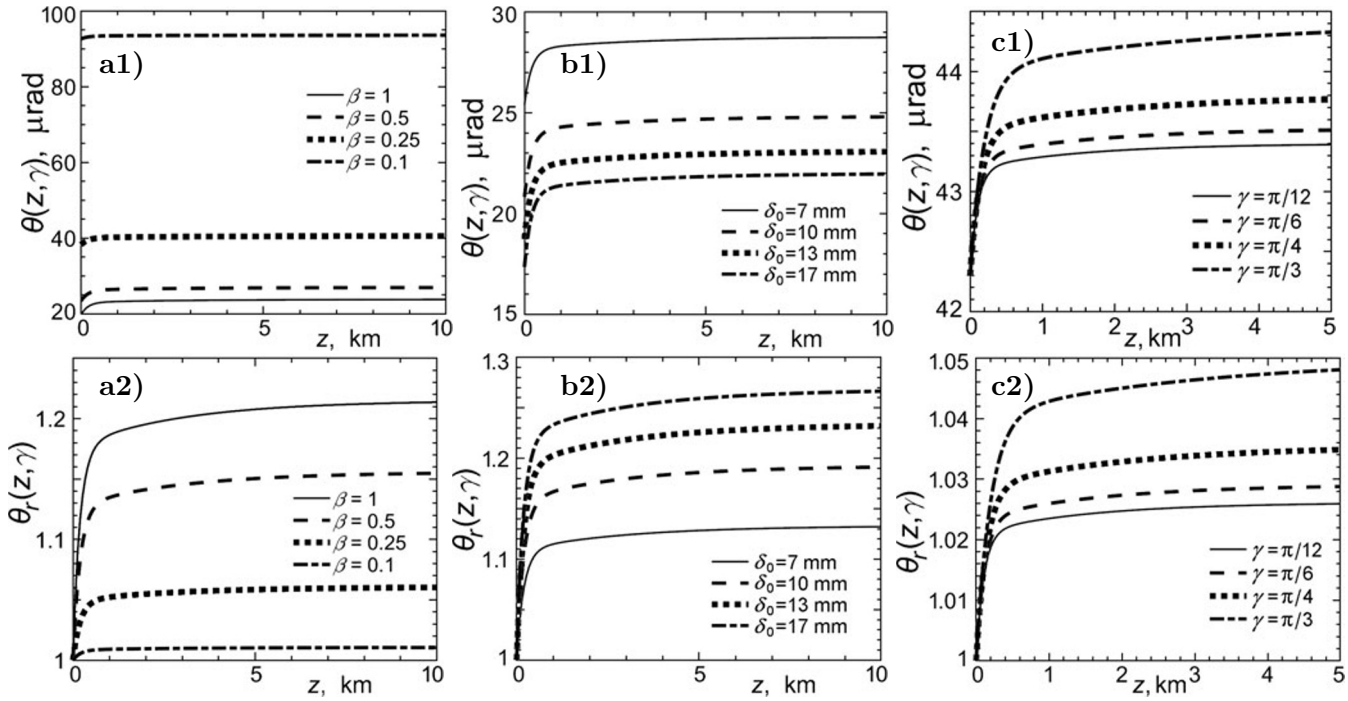


**Fig. 2.** The rms angular widths $\theta(z,\gamma)$ and the relative rms angular widths $\theta_r(z,\gamma)$ of PCTEVB under different ellipticity $\beta$, initial coherent lengths $\delta_0$, and zenith angle $\gamma$ versus the propagation distance through inhomogeneous turbulent atmosphere. Here, $m = 1$; also, $\mu_0 = 9 \cdot 10^{-4}$ m$^{-1}$, $\delta_0 = 1$ cm, and $\gamma = \pi/3$ (a1, a2); $\mu_0 = 4 \cdot 10^{-4}$ m$^{-1}$, $\beta = 0.25$, and $\gamma = \pi/3$ (b1, b2); $\beta = 0.25$, $\delta_0 = 5$ mm, and $\mu_0 = 8 \cdot 10^{-4}$ m$^{-1}$ (c1, c2).

The rms angular widths $\theta(z,\gamma)$ and relative rms angular widths $\theta_r(z,\gamma)$ of PCTEVB through inhomogeneous turbulent atmosphere under different beam parameters versus the propagation distance are shown in Fig. 2. As one can see, with increase in the propagation distance, the change trend of rms angular widths and relative rms angular widths increase rapidly and then trend to saturation. Therefore, this indicates that PCTEVB is less affected by the inhomogeneous atmospheric turbulence when propagates long distance. In Fig. 2 a1, a2, b1, b2, one can also find that the rms angular widths decrease with larger ellipticity and initial correlation lengths; however, the relative rms angular widths decreases with smaller ellipticity and initial correlation lengths. In Fig. 2 c1, c2, we can see that the zenith angle increases with increase in the both rms angular width and relative rms angular width.

In Fig. 3 a1, we see that the $M^2$-factor has a little change with increase in the propagation distance $z$; however, the $M^2$-factor is significantly influenced by the ellipticity, tending to increase with decreasing $\beta$.

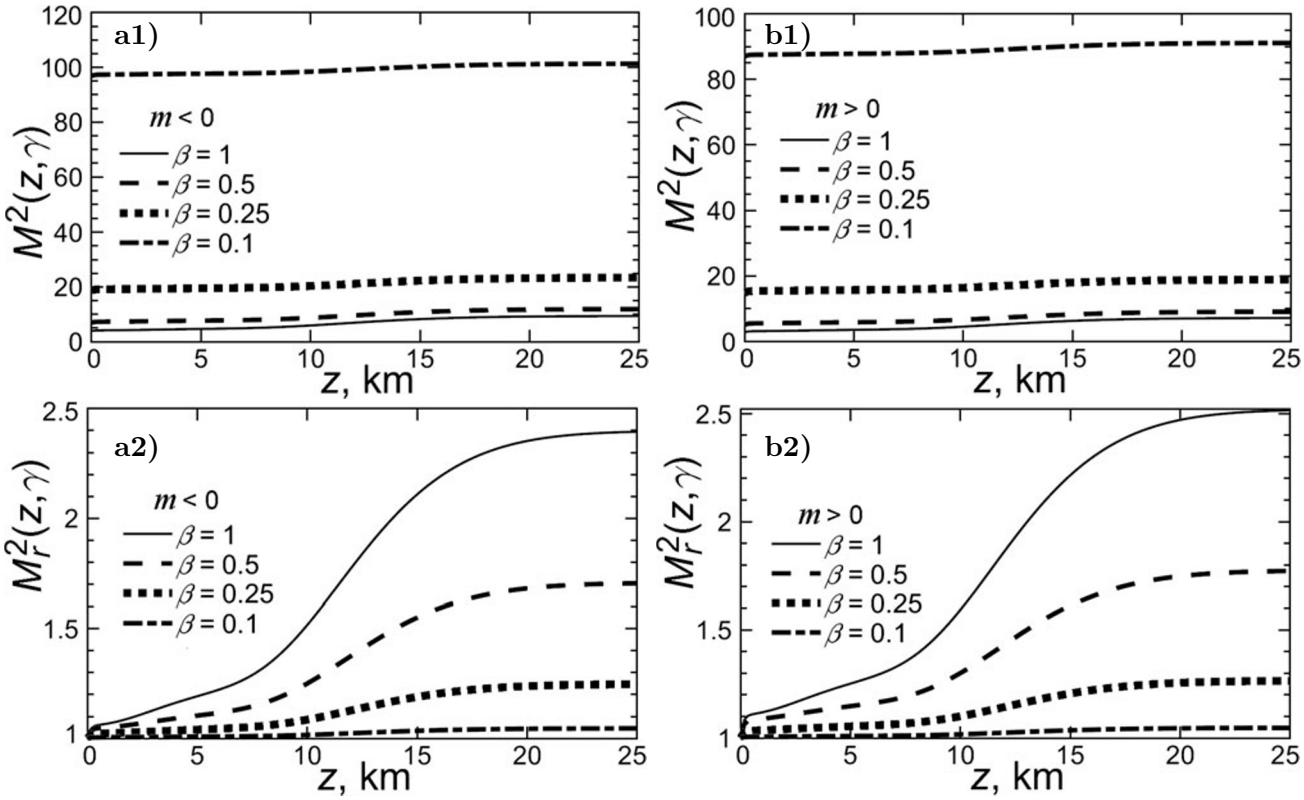


**Fig. 3.** The $M^2$-factor and the relative $M^2$-factor of PCTEVB versus the propagation distance through inhomogeneous turbulent atmosphere under different ellipticity $\beta$. Here, $\delta_0 = 1$ cm, $\mu_0 = 8 \cdot 10^{-4}$ m$^{-1}$, and $\gamma = \pi/12$.

In Fig. 3 a2, we can see that the smaller ellipticity leads to a lower relative $M^2$-factor; while the relative $M^2$-factor changes slowly when $z$ is smaller 10 km, but rapidly increases with increasing propagation distance $z$, eventually reaching a saturation. Furthermore, comparing Fig. 3 a1, a2 with Fig. 3 b1, b2, plus–minus of the topological charge $m$ is less affected by the $M^2$-factor and the relative $M^2$-factor of PCTEVB.

In Fig. 4, we show the $M^2$-factor and the relative $M^2$-factor of PCTEVB versus the propagation distance through inhomogeneous turbulent atmosphere under different twist factors $\mu_0$. In Fig. 4 a1, a2, we see that the $M^2$-factor increases with increase in the twist factor; however, the relative $M^2$-factor decreases with increase in the twist factor. Furthermore, when the propagation distance $z$ increases, the relative $M^2$-factor first increases slowly, then changes rapidly, and trends to saturation in the end; see Fig. 4 a2. Comparing Fig. 4 a1, a2 with Fig. 4 b1, b2, we can find that plus–minus of the twist factor $\mu_0$ is less affected by the $M^2$-factor and the relative $M^2$-factor. As is well known, when the topological charge and the twist factor have the same sign, they are said to have opposite chirality; on the contrary, they have the same chirality [12–15]. In Fig. 4 a2, b2, when they have some chirality, the relative $M^2$-factor is smaller. In other words, the better the beam quality of PCTEVB, the stronger the ability to resist turbulence.

In Fig. 5, we exhibit the $M^2$-factor and relative $M^2$-factor of PCTEVB versus the propagation distance through inhomogeneous turbulent atmosphere under different initial coherent lengths $\delta_0$ and the zenith angles $\gamma$. One can seen in Fig. 5 a1, a2 that, with decrease of the initial correlation lengths, the $M^2$-factor

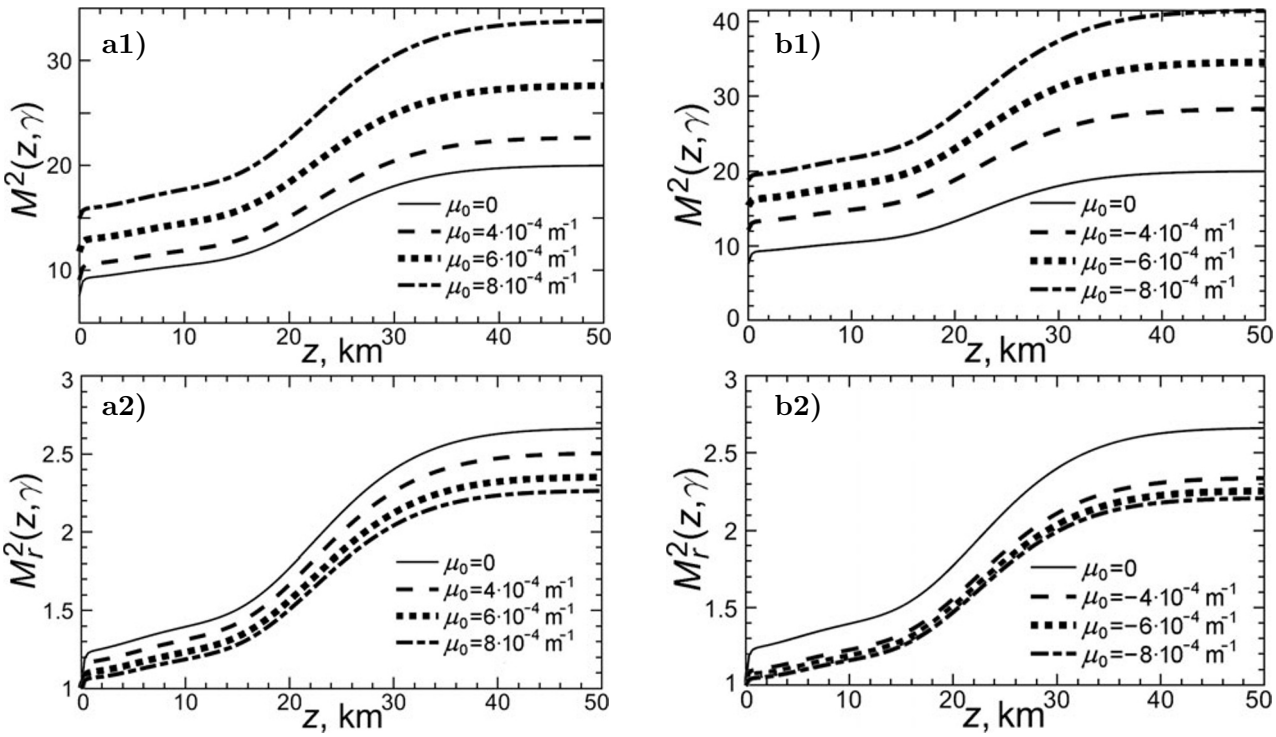


**Fig. 4.** The $M^2$-factor and the relative $M^2$-factor of PCTEVB versus the propagation distance through inhomogeneous turbulent atmosphere under different twist factors $\mu_0$. Here, $m = 1$, $\gamma = \pi/3$, $\beta = 0.25$, and $\delta_0 = 1$ cm.

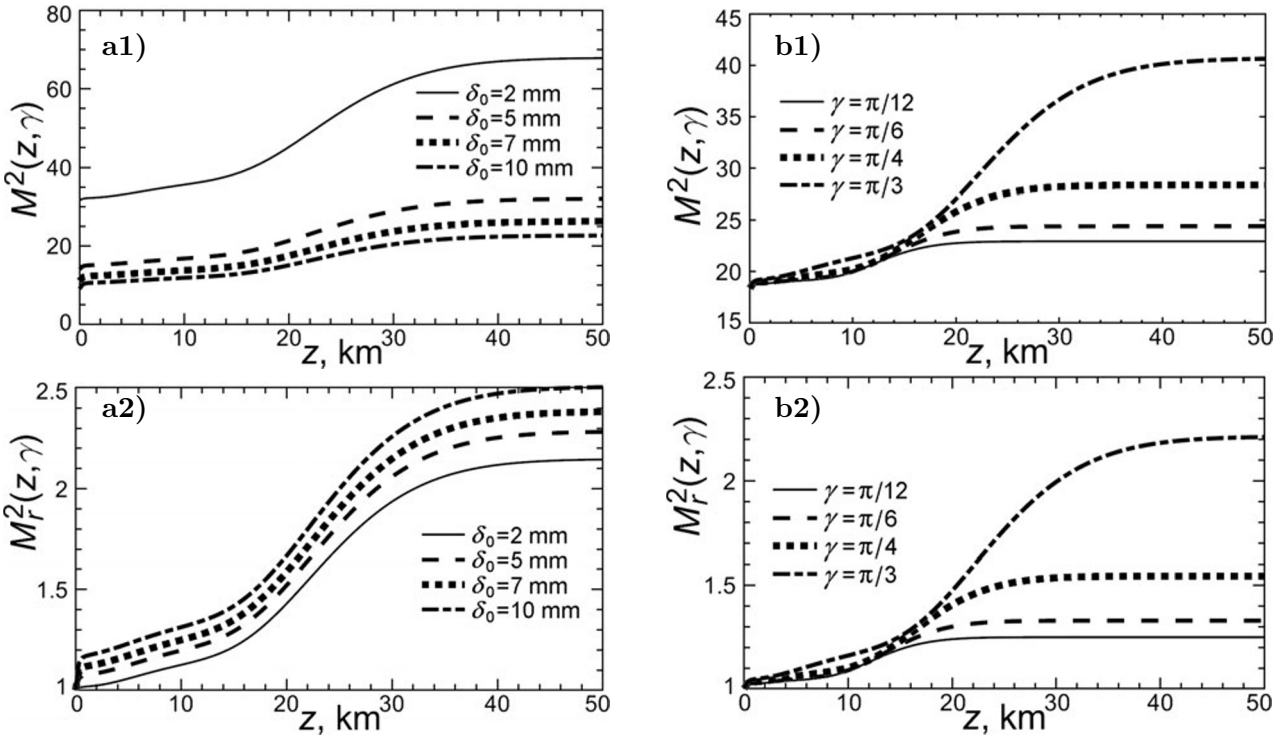


**Fig. 5.** The $M^2$-factor and relative $M^2$-factor of PCTEVB versus the propagation distance through inhomogeneous turbulent atmosphere under different initial coherent lengths $\delta_0$ and the zenith angle $\gamma$ at $\beta = 0.25$ and $m = 1$; here, $\gamma = \pi/3$ and $\mu_0 = 4 \cdot 10^{-4}$ m$^{-1}$ (a1, a2); $\delta_0 = 5$ mm and $\mu_0 = 8 \cdot 10^{-4}$ m$^{-1}$ (b1, b2).

increases, and the relative $M^2$-factor decreases. The $M^2$-factor and the relative $M^2$-factor of PCTEVB increase with the increasing propagation distance $z$, and when $z > 40$ km, the $M^2$-factor and relative $M^2$-factor of PCTEVB tend to saturation, and the beam is almost not affected by atmospheric turbulence.

In Fig. 5 b1, b2, we can see that the larger the zenith angles, the larger $M^2$-factor and the relative $M^2$-factor of the beam; in other words, the smaller the zenith angle, the better the beam quality. That is because, as the zenith angle decreases and approaches vertical transmission, the change in $C_n^2$ becomes faster and reaches a weak turbulent regime. At this moment, the impact of turbulence on the accumulation of PCTEVB becomes weaker [5, 44, 47].

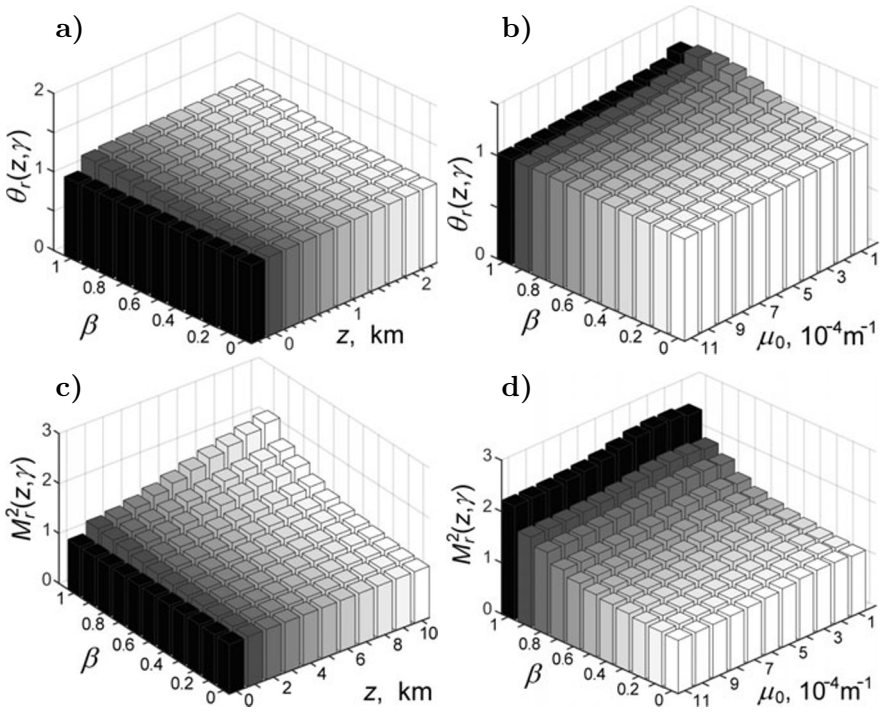


**Fig. 6.** The 3D relative $M^2$-factor and rm angular widths of PCTEVB through inhomogeneous turbulent atmosphere versus the propagation distance $z$ and ellipticity $\beta$ with the calculated parameters: $\delta_0 = 10$ mm, $\mu_0 = 8 \cdot 10^{-4}$ m$^{-1}$, and $\gamma = \pi/3$ (a, c) and versus the twist factor $\mu_0$ and ellipticity $\beta$ with the calculated parameters: $\delta_0 = 10$ mm, $z = 2$ km, and $\gamma = \pi/3$ (b, d).

In Fig. 6, we present the 3D relative $M^2$-factor and rm angular widths of PCTEVB through inhomogeneous atmospheric turbulence. As shown in Fig. 6 a, the relative rms angular widths are found to be less dependent on the propagation distance $z$. We also observe that the relative $M^2$-factor of PCTEVB in turbulence becomes saturated with increase in the propagation distance $z$; see Fig. 6 c. Furthermore, the smaller the ellipticity $\beta$ and the larger the twist factor $\mu_0$ contribute to decrease of the relative $M^2$-factor of PCTEVB; see Fig. 6 d. Comparing Fig. 6 b, d reveals that the relative rm angular widths follow the same change law as the relative $M^2$-factor. These outcomes suggest that the relative $M^2$-factor and relative rms angular widths are less affected by the inhomogeneous atmospheric turbulence.

In Fig. 7, we show the variation of the relative $M^2$-factor of PCTEVB with the propagation distance in inhomogeneous atmospheric turbulence under different topological charges. As seen in Fig. 7 a ,b, the relative $M^2$-factor decreases and the beam quality improves with increase in the topological charge $m$. Moreover, a comparison between Fig. 7 a, b reveals that the relative $M^2$-factor is smaller, when the ellipticity $\beta$ is smaller. This further verifies the rule obtained in Fig. 3 that the smaller the ellipticity $\beta$, the smaller the relative $M^2$-factor, indicating a stronger anti-turbulence ability of PCTEVB.

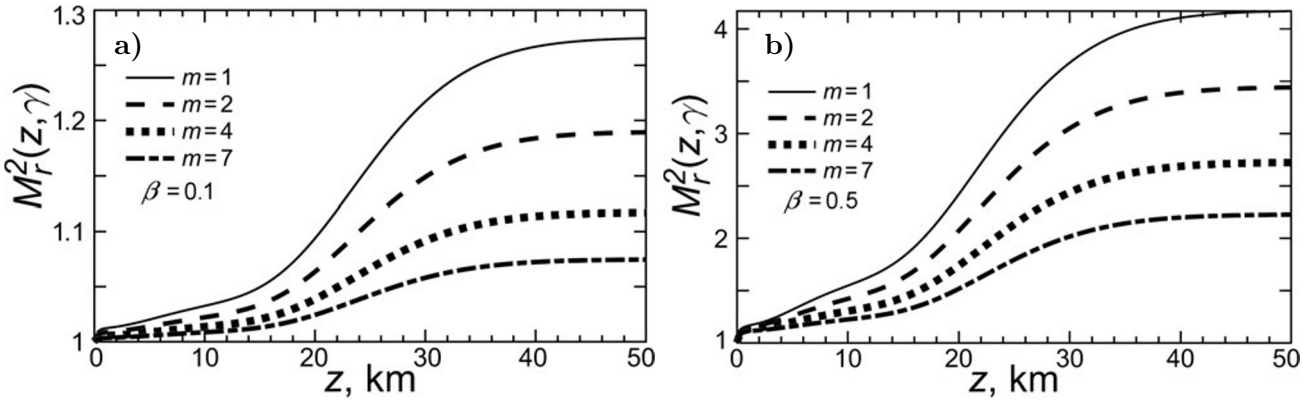


**Fig. 7.** The relative $M^2$-factor of PCTEVB versus the propagation distance through inhomogeneous turbulent atmosphere under different topological charge $m$. Here, $\gamma = \pi/3$, $\mu_0 = 8 \cdot 10^{-4}$ m$^{-1}$, and $\delta_0 = 10$ mm; also, $\beta = 0.1$ (a) and $\beta = 0.5$ (b).

## 4. Summary

In this paper, we first derived the analytical formulas for the spatial spreading, rms angular width, and the $M^2$-factor through the inhomogeneous atmospheric turbulence, using the extended Huygens–Fresnel principle and the second-order moment of the the Wigner distribution function. Then, we analyzed PCTEVB under different beam parameters versus the propagation distance through inhomogeneous turbulent atmosphere. The rms spatial width, rms angular width, and $M^2$-factor of PCTEVB in turbulence depend on the topological charge $m$, the ellipticity $\beta$, the initial coherent lengths $\delta_0$, the twist factor $\mu_0$, the zenith angle $\gamma$, and the propagation distance $z$.

We found that the relative rms spatial width, rms angular width, and $M^2$-factor of PCTEVB are smaller with decrease of the ellipticity $\beta$. We also obtained that the relative rms spatial width and the $M^2$-factor of PCTEVB are less affected by the turbulence with larger $\mu_0$ and smaller $\delta_0$; the relative rms angular width and the $M^2$-factor of PCTEVB are less affected by the turbulence with smaller $\delta_0$ and $\gamma$. In addition, the PCTEVB through the turbulence has strong anti-turbulence ability when it propagates with long distance. In the end, relative $M^2$-factor decreases with increase in the topological charge $m$. Our numerical results indicate that PCTEVB can mitigate atmospheric effects and may be useful for related applications.

## Acknowledgments

This work is supported by the Department of Science and Technology of Sichuan Province under Grants Nos. 2021YJ0518 and 2019YJ0470, the Sichuan Provincial University Key Laboratory of Detection and Application of Space Effect in Southwest Sichuan under Grant No. ZDXM202201003, the National Natural Science Foundation of China (NSFC) under Grant No. 11703011, and the Yunnan Key Laboratory of Solar Physics and Space Science under Grant No. YNSPCC202202.

## References

1. Manisha, S. Joshi, S. N. Khan, et al., *Opt. Express*, **30**, 32230 (2022).

2. S. N. Khan, S. Joshia, B. Kanseri, et al., *Appl. Phys. Lett.*, **118**, 051104 (2021).
3. Q. Xu, L. Zhao, and Y. G. Xu, *Optik*, **265**, 169542 (2022).
4. H. Zhang, H. Y. Wang, X. Y. Lu, et al., *Opt. Express*, **30**, 29923 (2022).
5. K. Huang, Y. G. Xu, L. Zhao, et al., *Optik*, **271**, 170247 (2022).
6. Y. Xu, Y. G. Xu, S. J. Wang, et al., *J. Russ. Laser Res.*, **43**, 509 (2022).
7. Z. H. Yang, H. Y. Wang, Y. H. Chen, et al., *Opt. Lett.*, **47**, 4467 (2022).
8. L. Zhao, Y. G. Xu, and S. K. Yang, *Optik*, **227**, 166115 (2021).
9. D. J. Liu, Y. C. Wang, and H. M. Yin, *Appl. Opt.*, **54**, 10510 (2015).
10. D. M. Wei, S. W. Li, J. Zeng, et al., *J. Russ. Laser Res.*, **41**, 364 (2020).
11. R. Simon and N. Mukunda, *J. Opt. Soc. Am. A.*, **10**, 95 (1993).
12. L. X. Liu, H. Y. Wang, L. Liu, et al., *Opt. Express*, **30**, 7511 (2022).
13. S. A. Wadood, K. V. Liang, Y. Y. Zhou, et al., *Opt. Express*, **29**, 22034 (2021).
14. Y. Zhang, X. Zhang, H. Y. Wang, et al., *Opt. Express*, **29**, 41964 (2021).
15. Y. Q. Zhou, Z. W. Cui, and Y. P. Han, *Opt. Express*, **30**, 23448 (2022).
16. R. Simon and N. Mukunda, *J. Opt. Soc. Am. A.*, **15**, 2373 (1998).
17. G. F. Wu, *J. Opt. Soc. Am. A.*, **33**, 345 (2016).
18. A. T. Friberg, E. Tervonen, and J. Turunen, *J. Opt. Soc. Am. A.*, **11**, 1818 (1994).
19. E. Razueva and E. Abramochkin, *J. Opt. Soc. Am. A.*, **36**, 1089 (2019).
20. W. H. Du, Z. Y. Yang, Z. Jin, et al., *J. Russ. Laser Res.*, **41**, 278 (2020).
21. L. Allen, M. W. Beijersbergen, R. J. C. Spreeuw, et al., *Phys. Rev. A*, **45**, 8185 (1992).
22. S. A. Ponomarenko, *Opt. Soc. Am. A.*, **39**, C1 (2022).
23. J. F. Xie, H. M. Guo, S. L. Zhuang, et al., *Opt. Express*, **29**, 3081 (2021).
24. T. R. Bai, Q. Li, Y. Q. Wang, et al., *Opt. Express*, **29**, 25270 (2021).
25. S. J. Zheng, H. J. Liu, Y. Lin, X. et al., *Opt. Express*, **29**, 43193 (2021).
26. W. Tan, Y. F. Bai, X. W. Huang, et al., *Opt. Express*, **30**, 14061 (2022).
27. Z. H. Pei, S. J. Huang, Y. Chen, et al., *J. Mod. Opt.*, **68**, 224 (2021).
28. Y. F. Du, D. M. Liu, S. N. Fu, et al., *Opt. Express*, **29**, 17353 (2021).
29. S. N. Khonina and A. P. Porfirev, *Optik*, **229**, 166299 (2021).
30. L. J. Yang and J. S. Li, *Opt. Express*, **30**, 36960 (2022).
31. J. N. He, M. L. Wan, X. P. Zhang, et al., *Opt. Express*, **30**, 4806 (2022).
32. G. Gbur and R. K. Tyson, *J. Opt. Soc. Am. A.*, **25**, 225 (2008).
33. J. I. Davis, *Appl. Opt.*, **5**, 139 (1966).
34. M. Segel and S. Gladysz, *Opt. Express*, **29**, 805 (2021).
35. L. Zhao, Y. G. Xu, and Y. Q. Dan, *Opt. Express*, **29**, 34986 (2021).
36. L. Zhao, Y. Xu, N. Yang, et al., *J. Opt. Soc. Am. A.*, **38**, 1255 (2021).
37. Y. Xu, L. Zhao, N. Yang, et al., *J. Mod. Opt.*, **69**, 200 (2022).
38. Z. Q. Zhong, X. Zhang, B. Zhang, et al., *Opt. Express*, **30**, 24421 (2022).
39. Y. G. Xu, Y. D. Li, and X. L. Zhao, *J. Opt. Soc. Am. A.*, **32**, 1623 (2015).
40. J. Cheng, *Opt. Express*, **17**, 7916 (2009).
41. L. Wang, J. Wang, C. J. Yuan, et al., *Optik*, **218**, 165037 (2020).
42. V. V. Kotlyar, A. A. Kovalev, and A. P. Porfirev, *Phys. Rev. A.*, **95**, 053805 (2017).
43. Y. K. Wang, L. Bai, J. Y. Xie, et al., *Opt. Express*, **29**, 16056 (2021).
44. T. Yang, Y. G. Xu, H. H. Tian, et al., *J. Opt. Soc. Am. A.*, **34**, 713 (2017).
45. Y. Q. Dan and B. Zhang, *Opt. Express*, **16**, 15563 (2008).
46. Y. G. Xu, Y. Q. Dan, J. Y. Yu, et al., *J. Mod. Opt.*, **64**, 1976 (2017).
47. K. Huang, Y. G. Xu, J. Cao, et al., *J. Russ. Laser Res.*, **44**, 110 (2023).